Supplemental Document

Optics Letters

Evolution of optical vortices in gradient media and curved spaces: supplement

YUHANG YIN,[1,2,†] QILIN DUAN,[1,2,†] JING LI,[1] CHENGWEI QIU,[2] AND HUANYANG CHEN[1,3,*]

[1] *Pen-Tung Sah Institute of Micro-Nano Science and Technology and Department of Physics, Xiamen University, Xiamen 361005, China*
[2] *Department of Electrical and Computer Engineering, National University of Singapore, Singapore 117583, Singapore*
[3] *Shenzhen Research Institute of Xiamen University, Shenzhen 518000, China*
[†] *These authors contributed equally to this Letter.*
[*] *Corresponding author: kenyon@xmu.edu.cn*

Supplement DOI: https://doi.org/10.6084/m9.figshare.21713933

Parent Article DOI: https://doi.org/10.1364/OL.472963

Evolution of optical vortices in gradient media and curved spaces

YUHANG YIN,[1,3] QILIN DUAN,[1] JING LI,[1] CHENGWEI QIU,[3] AND HUANYANG CHEN[1,2,*]

[1] Pen-Tung Sah Institute of Micro-Nano Science and Technology and Department of Physics, Xiamen University, Xiamen 361005, China
[2] Shenzhen Research Institute of Xiamen University, Shenzhen 518000, China.
[3] Department of Electrical and Computer Engineering, National University of Singapore, Singapore 117583, Singapore
** e-mail: kenyon@xmu.edu.cn*

Received XX Month XXXX; revised XX Month, XXXX; accepted XX Month XXXX; posted XX Month XXXX (Doc. ID XXXXX); published XX Month XXX

1. Methods (Numerical Simulations)

We perform simulations using the commercial software COMSOL Multiphysics. In 2D MFE mirror lenses, we perform the ray trajectories simulations using geometrical optics module. The vortex source is radiated from a circle with a radius of $\boldsymbol{r_1}(\boldsymbol{r_1} > \boldsymbol{r_0} = \boldsymbol{l}/\boldsymbol{k})$, illustrated by 16 rays. $\boldsymbol{l}$ is the topological charge and $\boldsymbol{k} = \mathbf{2}\boldsymbol{\pi}/\boldsymbol{\lambda}$(wavelength) is the wavenumber. From Berry's theory [1], the rays show tight spiraling inside the circle $\boldsymbol{r} = \boldsymbol{r_0}$, while radiating outwards with the lines asymptotically tangent to the circle $\boldsymbol{r} = \boldsymbol{r_0}$. Hence, with enough big radiating radius, we can simulate the azimuthal vortex flow by add extra angle $\boldsymbol{\varphi_0} = \mathbf{arctan}\,(\boldsymbol{l}/\boldsymbol{r})$. The background refractive profiles are given as $\boldsymbol{n_{rm}} = \mathbf{2}\boldsymbol{r}^{(\boldsymbol{m}-\mathbf{1})}/(\mathbf{1} + \boldsymbol{r}^{\mathbf{2}\boldsymbol{m}})$, where *m* is 1 or 2, and the mirror is added at the boundary in simulations.

Next, we use wave optics module to perform the full wave simulations. As is known, the MFE lens is only valid for transverse electric (TE) polarized wave, and consequently, perfect electric conductor (PEC) is chosen as the mirror boundary in full wave simulations. For a finite MFE lens, the symmetric refractive index profile and mirror boundary will form a pair of source and image points with center symmetry. Here, the background vortex source can be given as: $\boldsymbol{\psi}(\boldsymbol{r},\boldsymbol{l}) = \boldsymbol{H_l^{(1)}}(\boldsymbol{k_0} * \boldsymbol{r})\mathbf{exp}\,(\boldsymbol{il\varphi})$ with only z component of electric field, $\boldsymbol{k_0}$ is wavenumber in air and $\boldsymbol{\varphi}$ is the azimuth angle. The given form of vortex source can be realized by using *N* line currents surrounding a circle, with a phase difference of $\mathbf{2}\boldsymbol{l\pi}/\boldsymbol{N}$. For $\boldsymbol{l}$=1, we can simply use 4 line currents in simulations. The radius of the MFE lens is about seven times of the wavelength, while the radius of CPA is one-fifteenth wavelength. Furthermore, the parameter of CPA can be obtained using Mie scattering theory [2,3] and numerical methods. The design principle of CPA allows us to adjust the order *l* of the functions for satisfying excitations carrying different TCs *l*. The value of CPA is dependent on the position in MFE lenses because of the gradient refractive index profile. Here, for a fixed position in the main text, the values of CPAs are $\boldsymbol{n_{m=1}} = \mathbf{5.53} + \mathbf{0.505}\boldsymbol{i}$ and $\boldsymbol{n_{m=2}} = \mathbf{5.59} + \mathbf{0.208}\boldsymbol{i}$ respectively.

In 3D GLs, the electric field are confined in the PEC waveguide filled with air with a thickness *t* of one tenth of the wavelength, as shown in Fig. 4(a). The sphere and spindle have the same thickness *t*. We set the shell boundary as PEC and plot the z component of the electric field at the outer surface of GLs. The vortex source here can be realized by using *N* electric point dipoles feeding with different phases the same as 2D cases. For sphere, any incidence will form a corresponding image located at the opposite of sphere, and the two points are symmetrical about the equator. Thus, the value of CPA here is constant. The CPA here has the same radius in 2D cases and the value is $\boldsymbol{n_{M=1}} = \mathbf{7.49} + \mathbf{0.184}\boldsymbol{i}$. For spindle, the source and image point are still symmetrical about the center plane, but with a vary distance when change the source position along *x* axis. Consequently, this will lead to a different value of CPA due to the difference of effective refractive index. Here, we emit vortex source inside the air layer at a distance of 1m to the center plane along *x* axis, and the value of CPA is set as $\boldsymbol{n_{M=2}} = \mathbf{7.47} + \mathbf{0.233}\boldsymbol{i}$.

2. Imaginary part of Electric field

In this section, we present the results of the imaginary part of the electric field in GMFE lenses and on GLs. In Fig. S1, we present the results with CPA all positions in GMFE lenses. Here, S denotes vortex source and C (1,2) denotes the converge point or CPA. From the results we obtained both 2D and 3D cases shown in Fig. S1 and S2, it can be found that the difference between the real and imaginary part of electric field is phase shift only. Meanwhile, the vortex cannot be reconstructed without the aid of CPAs.

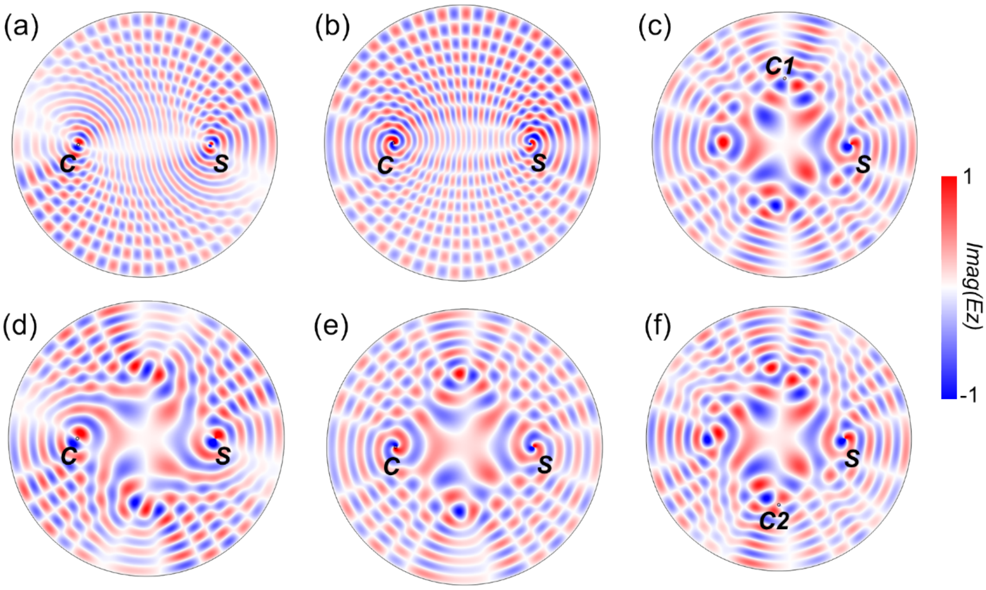

FIG. S1. Imaginary part of electric field in GMFE lens with vortex emission. Vortex emission in MFE lens (a) without CPA and (b) with CPA. Vortex emission in GMFE lens (d) without CPA and (c) with CPA at C1 point, (e) C point and (f) C2 point.

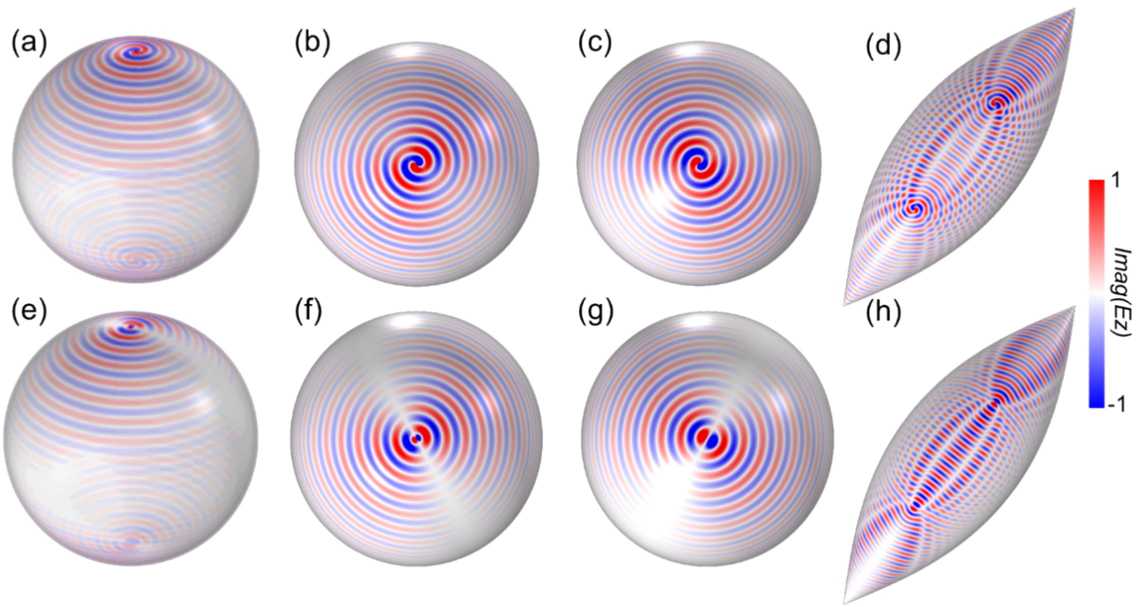

FIG. S2. Imaginary part of electric field on GLs. Vortex on sphere (a) with CPA and (e) without CPA, where (b-c) and (f-g) are two views from the north and south pole, respectively. Vortex on spindle (d) with CPA and (h) without CPA.

3. Variations of the vortex source and CPA positions

In this section, we present the results of changing the original emission position of vortex and the corresponding CPA positions. In Fig. S3(a-f), we show the two positions that are closer to (x=R/3) or away from (x=3R/4) the center compared with the results shown in the main text (x=R/2). In the above positions, we can also observe the reconstruction of the vortex in the converging position with the aid of CPAs. Due to the rotation symmetry of the refractive index profile, thus one can rotate the source and CPA simultaneously to a random degree. However, if we fixed the position of vortex source, we will not be able to recover the vortex when changing the positions of CPAs, as shown in Fig. S3(g-h). In 3D cases, we first discuss the sphere. Due to the symmetry of sphere surface, one can arbitrarily rotate the source and CPA simultaneously without destroy the reconstruction of the vortex. However, if we fix the source position and then rotate the CPA only, we cannot observe the reconstruction of vortex on sphere with the two arbitrary positions shown in Fig. S4(a-b), similar with the 2D cases. For spindle, we first move the CPA only, slightly deviate from the converging position. We find the vortex cannot be recovered, as shown in Fig. S4(c). Instead, we put the vortex source and CPA correspondingly at a distance of 1.5m to the center plane along x axis (away from the distance in the main text), and we can still observe the reconstruction of vortex. Actually, one may get the answer ahead through Fig. 2(c) shown in the main text, where the C1 position cannot recover the vortex. To conclude, the observation position is only valid in the fully converging position shown in the ray trajectories, where the vortex information is lossless.

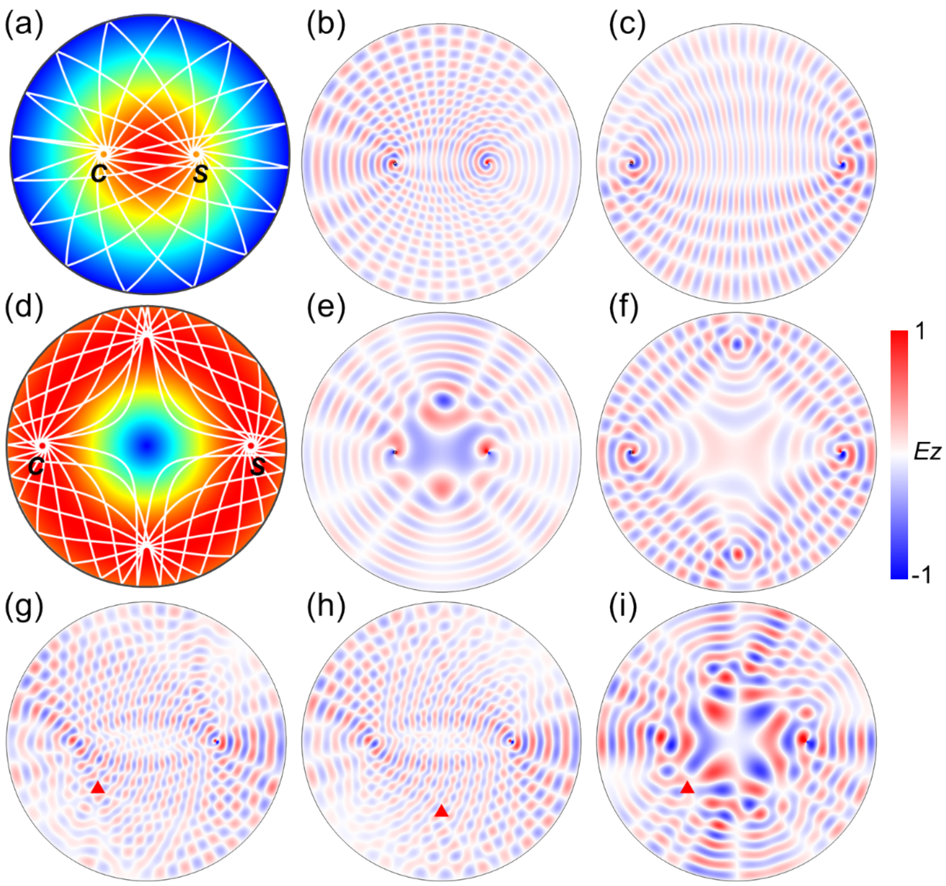

FIG. S3. Variations of the vortex source and CPA positions in GMFE lenses. (a) Ray tracing of the vortex emission located at x=R/3 in MFE lens. (d) Ray tracing of the vortex emission located at x=3R/4 in GMFE lens. Vortex electric field emission at the two positions (b-c) in MFE lens and (e-f) in GMFE lens with CPAs.

(g-i) Arbitrary CPA placements (marked as the red triangle) in GMFE lenses. The center of the device is coordinate origin, and the radius is *R*.

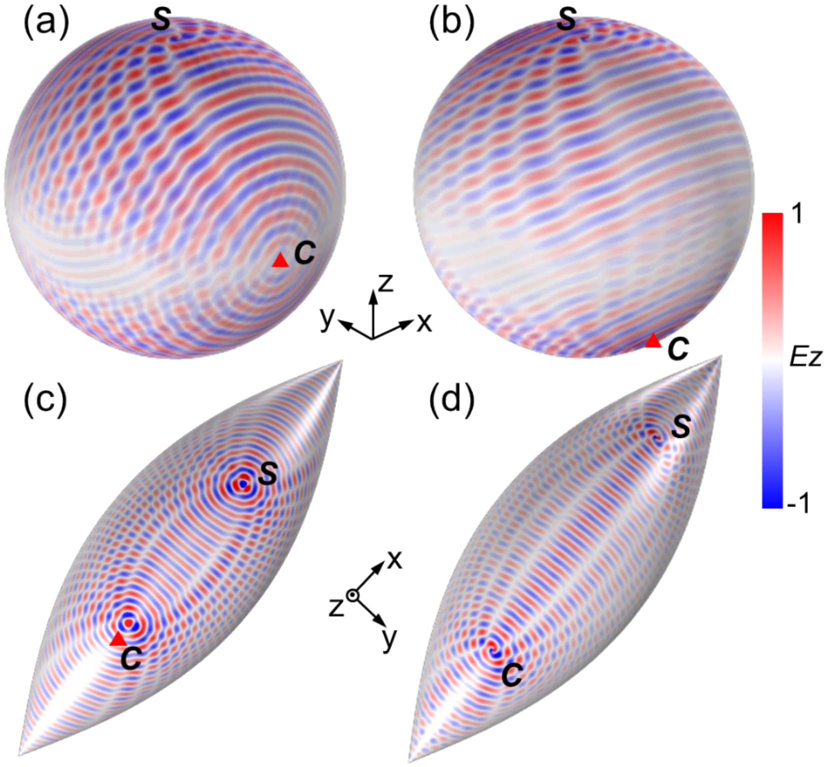

FIG. S4. Variations of the vortex source and CPA positions on GLs. Vortex on sphere with CPA at a distance of (a) quarter circle and (b) three-eighths circle between source. Vortex on spindle with CPA (c) slightly deviate from the converging point along *x* axis and (d) at a new distance of *x*=1.5m. Here, S presents the vortex source and C presents the CPA (also marked as red triangle).

References

1. M. Berry, J. Opt. **15**, 044006 (2013).
2. H. Noh, Y. Chong, A. D. Stone, and H. Cao, Phys. Rev. Lett. **108**, 186805 (2012).
3. L. Xu, and H. Chen, EPL (Europhysics Letters) **100**, 34001 (2012).